

# $e^+$ and $\bar{p}$ from inert doublet model dark matter

Emmanuel Nezri<sup>1</sup>, Michel H.G. Tytgat<sup>2</sup>, Gilles Vertongen<sup>2</sup>

<sup>1</sup>*Laboratoire d'Astrophysique de Marseille, OAMP,  
Technopôle de Marseille-Etoile. 38, rue Frédéric Joliot-Curie 13388 Marseille, France*

<sup>2</sup>*Service de Physique Théorique, Université Libre de Bruxelles,  
CP225, Bld du Triomphe, 1050 Brussels, Belgium*

## Abstract

We investigate the signatures of antimatter in cosmic rays that would result from annihilations of the scalar dark matter candidate of the Inert Doublet Model. We consider three benchmark candidates, all consistent with the WMAP cosmic abundance and existing direct detection experiments, and confront the predictions of the model with the recent PAMELA, ATIC and HESS data. For a light IDM WIMP candidate,  $M_{DM} = 10$  GeV, we argue that the positron and antiproton fluxes are large, but consistent with expected backgrounds, unless there is an enhancement in the local density of dark matter. For an IDM WIMP candidate with  $M_{DM} = 70$  GeV, the contribution is lower than the expected backgrounds unless there is a large boost factor. However, the candidate is able to explain the excesses observed by the recent experiments. Finally, for an IDM WIMP candidate with  $M_{DM} = 10$  TeV, it is possible to fit the PAMELA excess, while satisfying the anti-protons data, but, unfortunately, not the ATIC one.

## 1 Introduction

Cosmological observations indicate that about 80% of matter in the universe is dark matter (DM) [1–3]. The most popular particle physics explanation for DM is that it is made of weakly interacting massive particles or WIMPs [4, 5]. The prominent WIMP candidate is the neutralino, a spin 1/2 Majorana particle, but spin one (like in models with extra dimensions [6]) and, to lesser extent, scalars particles are considered as interesting challengers. An instance of the latter is the lightest stable scalar of the Inert Doublet Model (IDM), an extension of the Standard Model with two Higgs doublets and a discrete  $Z_2$  symmetry introduced to prevent FCNC [7]. The scope and ambition of the IDM can not compete with those of the MSSM or models with extra dimensions but the model does have an interesting phenomenology, emphasized in [8, 9] and *e.g.* [10]. Also, it encompasses some features of other models with scalar dark matter, like Minimal Dark Matter [11] or singlets like in hidden portal models [12, 13].

The prospects for direct and indirect detection through gamma rays from the Galactic Centre (GC) or neutrinos from the Earth and Sun have been addressed in [9, 14–18]. We study in the present article the production and propagation of positrons and anti-protons from annihilations of the IDM dark matter candidate<sup>1</sup>. The subject matter is timely, given the release of observations by the Payload for Antimatter Exploration and Light-Nuclei Astrophysics (PAMELA), which show an excess of positrons in the 10 – 80 GeV range [20] (and no excess in the antiproton over proton flux [21]), and, even more recently by the Advanced Thin Ionization Calorimeter (ATIC), which shows an excess of cosmic ray electrons at energies of 300 – 800 GeV [22]. At higher energies, 600 GeV – 4 TeV, the High Energy Stereoscopic System (HESS), an array of Cerenkov telescopes, has measured the background flux of cosmic ray electrons (plus positrons) [23].

There has been a flurry of activity on antimatter production, both from a model independent point of view [24–28] and on building models of DM [29–31]. There are good and simple reasons why the IDM can not

<sup>1</sup>For a summary on the search of dark matter, including the IDM candidate, see [19].

pretend to be able to fully explain the recent data. However there is no analysis yet of antimatter production in the IDM and we see this as an opportunity to both fill a gap in the literature.

The paper is organized as follow. The Inert Doublet Model is summarized in Section 2. Anti-protons and positrons productions and propagations are briefly tackled within Section 3, together with a discussion on background estimations. Section 4 is devoted to the putative contribution of IDM dark matter annihilations to cosmic rays. Cosmic rays features specific of the Inert Doublet Model and, in particular, their relevance for the results of PAMELA, ATIC and HESS experiments are presented in Section 5. Conclusions are given in Section 6.

## 2 The Inert Doublet Model

The Inert Doublet Model is a two Higgs doublet model,  $H_1$  and  $H_2$ , with an unbroken  $Z_2$  symmetry such that

$$H_1 \rightarrow H_1 \text{ and } H_2 \rightarrow -H_2.$$

and with all the other Standard Model particles even [8, 9]. The potential of the IDM can be written as

$$V = \mu_1^2 |H_1|^2 + \mu_2^2 |H_2|^2 + \lambda_1 |H_1|^4 + \lambda_2 |H_2|^4 + \lambda_3 |H_1|^2 |H_2|^2 + \lambda_4 |H_1^\dagger H_2|^2 + \frac{\lambda_5}{2} \left[ (H_1^\dagger H_2)^2 + h.c. \right]. \quad (1)$$

In this model,  $H_1$  contains the standard Brout-Englert-Higgs particle  $h$  (the Higgs for short) and the discrete symmetry, which prevents FCNC, gives a dark matter candidate in the form of one of the neutral components of the extra doublet  $H_2 = (H^+, 1/\sqrt{2}(H_0 + iA_0))^T$

$$\begin{aligned} M_h^2 &= -2\mu_1^2 \equiv 2\lambda_1 v^2 \\ M_{H^+}^2 &= \mu_2^2 + \lambda_3 v^2 / 2 \\ M_{H_0}^2 &= \mu_2^2 + (\lambda_3 + \lambda_4 + \lambda_5) v^2 / 2 \\ M_{A_0}^2 &= \mu_2^2 + (\lambda_3 + \lambda_4 - \lambda_5) v^2 / 2 \end{aligned} \quad (2)$$

Depending on quartic couplings, either  $H_0$  or  $A_0$  can be the lightest particle. We choose  $H_0$  and, following [9], we define  $\lambda_L = (\lambda_3 + \lambda_4 + \lambda_5)/2$ , coupling between  $h$  and a pair of  $H_0$ . In our investigation of the model we choose  $\mu_2$ ,  $\lambda_2$  and the masses of scalar particles, including the mass of the Higgs, as input parameters.

Experimental constraints on the IDM model are discussed in [9] and further in [32] and [33]. The latter also discuss the prospect for discovery of the  $A_0$  and  $H_0$  at the LHC. In [32] the LEP I and II constraints on the neutralino are used to put constraints on the mass range of  $H_0$  and  $A_0$ , see in particular their Fig.8. In the present work, we consider that  $H_0$  is the dark matter candidate. The  $A_0$  masses (and that of  $H^\pm$ ) we will use are always consistent with LEP and WMAP data.

Assuming that  $H_0$  were in thermal equilibrium in the early universe, there are essentially three distinct  $H_0$  mass ranges that are consistent with the WMAP abundance for dark matter. In the sequel we refer to them as the low mass ( $3 \text{ GeV} \lesssim M_{H_0} \lesssim 8 \text{ GeV}$ ), the middle mass ( $40 \text{ GeV} \lesssim M_{H_0} \lesssim 80 \text{ GeV}$ ) and the high mass ( $500 \text{ GeV} \lesssim M_{H_0} \lesssim 15 \text{ TeV}$ ) ranges. Candidates in the low mass range annihilate only through the Higgs channel. These solutions are challenged, but not excluded, by current direct detection experiments (CDMS, Xenon and Cogent) and may be compatible with the DAMA result [17]. Candidates in middle mass range may annihilate in the  $Z$  (when coannihilation with  $A_0$  is kinematically allowed) or the Higgs channel. Some solutions may give a very significant gamma ray line from annihilation at the GC. This line might be observed by the GLAST/Fermi satellite [15]. Above 80 GeV, annihilation into  $W^\pm$  pairs is allowed, the cross section is large and the abundance falls well below the WMAP abundance [14]. At higher masses, the annihilation cross section tend to decrease and the relic abundance increases. This regime is analogous to that of Minimal Dark Matter [11] but, in the IDM case, there are more parameters to play with and there is a whole mass range around 1 TeV of candidates with an abundance consistent with WMAP [14].

### 3 Antimatter in Cosmic Rays

#### 3.1 Anti-protons

Anti-protons in cosmic rays are essentially secondaries and are created by spallation, through  $pp$  collisions that occur as cosmic rays travel through the Interstellar Medium (ISM). Creation, destruction and propagation of anti-protons in the ISM and galactic magnetic field may be described by a diffusion equation for the anti-proton density  $n_{\bar{p}}$ . Solving the equation requires the distributions of matters in the Galaxy which is generally modelled by two cylindrical slabs, one representing the position of the ISM gas and the other the halo of dark matter (see *e.g.* [34]). We take them to have radial extension  $R_g$  and heights  $2h_g$  and  $2h_h$  respectively. There are various models of anti-proton propagation and they all more or less in agreement with each others and with the existing data [34–37].

In the present article, to compute the flux of anti-protons at the top of the Earth atmosphere, we have used the propagation model implemented in the DarkSUSY package [38]. We have interfaced DarkSUSY with microMEGAs2.2 [39, 40], a versatile package that allow to compute the dark matter abundance (and the relevant branching ratios) of any WIMP dark matter candidate in models with a  $Z_2$  parity.

In DarkSUSY, stationary anti-protons densities satisfy the transport equation

$$\frac{\partial n_{\bar{p}}}{\partial t} = \nabla \cdot (D(R, \vec{x}) \nabla n_{\bar{p}}) - \nabla \cdot (\vec{u}(\vec{x}) n_{\bar{p}}) - p(E, \vec{x}) n(E, \vec{x}) + Q(E, \vec{x}) = 0. \quad (3)$$

Propagation is encompassed by the first three terms. The first ones describe diffusion in the galactic magnetic field. In each part of the Galaxy the diffusion coefficient  $D$  is assumed to be isotropic

$$D(\vec{x}) = D(z) = D_g \theta(h_g - |z|) + D_h \theta(|z| - h_g), \quad (4)$$

and to depend only on the magnetic rigidity parameter  $R$  of the anti-protons (in GigaVolts)

$$D_l(R) = D_l^0 \left(1 + \frac{R}{R_0}\right)^{0.6}, \quad (5)$$

where  $l = g, h$  and  $R_0 \sim 1 \text{ GV}$ . The second term represent large scale convective motion with velocity field  $\vec{u}(\vec{x})$ . It is introduced to model the impact of the wind of cosmic rays, that blows away from the disk, on the motion of anti-protons. The third term models the loss of anti-protons due to collision with the ISM, supposedly dominated by collisions with hydrogen,

$$p(E, \vec{x}) = n^H(\vec{x}) v(E) \sigma(E), \quad (6)$$

where  $\sigma$  is the inelastic cross section of the collision and  $n^H$  is the number density of hydrogen in the galaxy, which we assumed to be

$$n^H(\vec{x}) = n^H(z) = n_g^H \theta(h_g - |z|) + n_h^H \theta(|z| - h_g). \quad (7)$$

Finally the last term on the r.h.s. in (3) is the source of anti-protons with energy  $E$ ,  $Q(E, \vec{x})$ . Sources include (possibly) dark matter annihilations but also secondary anti-protons produced by spallation in protons collisions. Hence it is also necessary to solve a transport equation analogous to (3) for the proton density.

As for boundary conditions, it is assumed that the density of cosmic rays, and thus anti-protons, is negligible at the boundaries beyond the Galaxy, *i.e.*

$$n_{\bar{p}}(R_g, z) = n_{\bar{p}}(r, h_h) = n_{\bar{p}}(r, -h_h) = 0$$

To be able to discriminate between standard and exotic sources of anti-protons, it is necessary to have a good handle on the expected background signal. For the known astrophysical sources of anti-protons, the model sketched above gives a flux of anti-protons at moderate energies in very good agreement with observations, especially if  $p\text{-He}$  collisions in and energy losses during propagation are taken into account [37]. However, the lack of data for energies above 100 GeV implies an uncertainty on the propagation parameters

and the background flux is not uniquely determined [41]. For the sake of the argument, we use the background flux given in the analysis of [41]

$$\frac{d\phi}{dT_{\bar{p}}} = \frac{0.9 t^{-0.9}}{14 + 30 t^{-1.85} + 0.08 t^{2.3}} \quad [\text{GeV}^{-1} \cdot \text{m}^{-2} \cdot \text{s}^{-1} \cdot \text{sr}^{-1}] \quad (8)$$

where  $T_p \equiv E_{\bar{p}} - m_{\bar{p}}$  and  $t = T_{\bar{p}}/1 \text{ GeV}$ .

The anti-proton data are presented in term of the ratio of the anti-proton to proton fluxes,

$$\frac{\bar{p}}{p} \equiv \frac{d\phi/dT_{\bar{p}}}{d\phi/dT_p}$$

hence we need the flux of protons . This is given by [42]

$$\frac{d\phi}{dT_p} = \frac{0.9 t^{-1}}{8 + 1.1 t^{-1.85} + 0.8 t^{1.68}} \quad [\text{GeV}^{-1} \cdot \text{m}^{-2} \cdot \text{s}^{-1} \cdot \text{sr}^{-1}] \quad (9)$$

Typically the ratio  $\bar{p}/p$  observed is  $\mathcal{O}(10^{-4})$ .

### 3.2 Positrons

The pions and kaons created by spallation of primary nuclei are supposed to be the standard sources of positrons in cosmic rays. Positrons in turn loose their energy through synchrotron radiation in the interstellar magnetic field and through inverse Compton scattering on diffuse starlight and on the cosmic microwave background. We follow the treatment of [43].

The stationary positron number density per unit energy  $dn_{e^+}/dE_{e^+}$  is given by the solution of the transport equation

$$\frac{\partial}{\partial t} \frac{dn_{e^+}}{dE_{e^+}} = \vec{\nabla} \cdot \left[ K(E_{e^+}, \vec{x}) \vec{\nabla} \frac{dn_{e^+}}{dE_{e^+}} \right] + \frac{\partial}{\partial E_{e^+}} \left[ b(E_{e^+}, \vec{x}) \frac{dn_{e^+}}{dE_{e^+}} \right] + Q(E_{e^+}, \vec{x}), \quad (10)$$

where  $K(E_{e^+}, \vec{x})$  is the diffusion constant,  $b(E_{e^+}, \vec{x})$  is the rate of energy loss and  $Q(E_{e^+}, \vec{x})$  is the source term (in  $\text{cm}^{-3} \text{s}^{-1}$ ). The relation between the flux and the density number is

$$\frac{d\Phi}{dE_{e^+}} = \frac{\beta c}{4\pi} \frac{dn_{e^+}}{dE_{e^+}}. \quad (11)$$

Despite the fact that the distribution of stars in the Galaxy is not uniform, it is generally assumed that the diffusion constant is independent of position within a “diffusion zone”. Its energy dependence is given by

$$K(E) = K_0 \left[ C + \left( \frac{E}{E_0} \right)^\alpha \right], \quad (12)$$

where the diffusion coefficient at 1 GeV is  $K_0 = 3 \cdot 10^{27} \text{cm}^2 \text{s}^{-1}$ ,  $C = 3^\alpha$  implement a cutoff in the diffusion constant below 3 GeV and the spectral index is  $\alpha = 0.6$ . [43]. The energy loss rate depends on the positron energy through

$$b(E) = \left( \frac{E}{E_0} \right)^2 \frac{1}{\tau_E} \quad (13)$$

where  $\tau_E = 10^{16} \text{s}$  is the characteristic time for energy loss. The diffusion zone is modelled in this case by a slab of thickness  $2L$  with  $L = 3 \text{ kpc}$ . Only positrons coming from our nearest environment are contributing to the observable flux at the Earth, therefore this equation is solved by considering a leaky box model with free escape boundary conditions, *i.e.* the cosmic ray density goes to zero on the surfaces of the slab.

As for  $\bar{p}$ , to confront the putative contribution of dark matter annihilations to positrons in cosmic rays, we need a good handle on the expected  $e^+$  background. An extensive discussion of the (many) uncertainties on both  $e^+$  production by spallation and their subsequent propagation in the interstellar medium may be

found in [44]. A second issue is that to interpret the data it is also necessary to know the electron flux. This is because the positrons data are generally presented in term of the positron fraction

$$\frac{e^+}{e^+ + e^-} \equiv \frac{\frac{d\Phi}{dE} e^+}{\frac{d\Phi}{dE} e^+ + \frac{d\Phi}{dE} e^-}$$

Taking the ratio permits to factor out the energy dependence of the acceptance of the detectors, supposing it is the same for electrons and positrons. Incidentally, the electron flux spectrum is poorly known. For one thing it is difficult to simulate the  $e^-$  flux from first principles since there are many potential astrophysical sources of electrons. Also, the experimental situation is not ideal yet. A compilation of existing data is presented in [45]. The electron flux uncertainty impact on interpreting data of the positron flux is non-negligible, as discussed in [44]. We will come back to this issue in the next section. Concretely, in the present article, we follow [43] and use the following background flux of positrons and electrons

$$\left(\frac{d\Phi}{dE}\right)_{e^-, \text{ prim.}} = \frac{0.16 \epsilon^{-1.1}}{1 + 11 \epsilon^{0.9} + 3.2 \epsilon^{2.15}} \quad [\text{GeV}^{-1} \cdot \text{cm}^{-2} \cdot \text{s}^{-1} \cdot \text{sr}^{-1}] \quad (14)$$

$$\left(\frac{d\Phi}{dE}\right)_{e^-, \text{ sec.}} = \frac{0.70 \epsilon^{0.7}}{1 + 110 \epsilon^{1.5} + 600 \epsilon^{2.9} + 580 \epsilon^{4.2}} \quad [\text{GeV}^{-1} \cdot \text{cm}^{-2} \cdot \text{s}^{-1} \cdot \text{sr}^{-1}] \quad (15)$$

$$\left(\frac{d\Phi}{dE}\right)_{e^+, \text{ sec.}} = \frac{4.5 \epsilon^{0.7}}{1 + 650 \epsilon^{2.3} + 1500 \epsilon^{4.2}} \quad [\text{GeV}^{-1} \cdot \text{cm}^{-2} \cdot \text{s}^{-1} \cdot \text{sr}^{-1}] \quad (16)$$

where  $\epsilon = E/1\text{GeV}$ . As for  $\bar{p}$ , we compute the flux of positrons from IDM dark matter annihilation using DarkSUSY.

### 3.3 Solar modulation

Before closing this section, we mention that a further complication when confronting with data stems from the fact that low energy ( $E \lesssim 1 - 10$  GeV) cosmic rays (both  $e^+ - e^-$  and  $\bar{p} - p$ ) are strongly affected as they propagate in the solar system as they may loose energy by interacting with the solar wind and the magnetic field. These effects are generically called solar modulation. Standard practice is to assume that solar modulation is independent of the sign of charge and thus the same for electrons and positrons (for discussion see [43, 46]). Using the so-called Gleeson and Axford analytical force-field approximation [47, 48], the flux at the Earth  $d\Phi_{\oplus}/dE_{\oplus}$  can be deduced from the flux at the heliosphere boundary,  $d\Phi_{IS}/dE_{IS}$  by

$$\frac{d\Phi_{\oplus}}{dE_{\oplus}} = \frac{p_{\oplus}^2}{p_{IS}^2} \frac{d\Phi_{IS}}{dE_{IS}}, \quad (17)$$

where the energy at the heliospheric boundary is given by

$$E_{IS} = E_{\oplus} + |Ze|\phi, \quad (18)$$

and  $p_{\oplus}$  and  $p_{IS}$  are the momenta at the Earth and at the heliospheric boundary respectively,  $e$  is the absolute value of the electron charge, and  $Z$  is the charge of the particle in unit of  $e$ . The solar modulation is completely determined by the rigidity parameter  $\phi$ , *i.e.* the momentum divided by the charge,  $[\phi] = V$ . In first approximation, solar modulation is the same for positive and negative charge particles and thus its effect factors out when considering the  $e^+$  fraction or the ratio  $\bar{p}/p$ . Data have however become good enough to be sensitive to charge dependence solar modulation effects. In particular the recent PAMELA experiment has measured a substantially smaller positron fraction below 10 GeV than the previous experiments (essentially CAPRICE and HEAT [49–51]). Similarly, over the years, BESS has measured variations in the  $\bar{p}/p$  ratio. This charge dependent solar modulation effect is believed to be related to the inversion of the solar magnetic field polarity that takes place with a periodicity of 22 years, in phase with maximum of solar activity that occurs with every 11 years periodicity (see for instance [52] and [53]). However, for the time being, there seems to be no complete understanding of solar modulation effects. This somehow limits the use we could make of low energy data (both on  $e^+$  and  $\bar{p}$ ) to constraint models of dark matter. However we will try to argue otherwise.

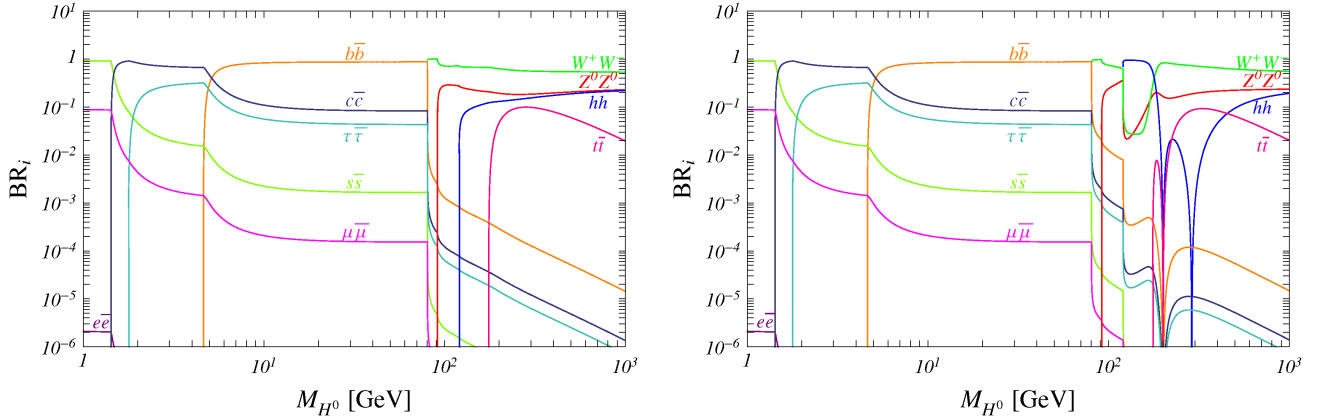


Figure 1: Branching ratios of the  $H_0$  annihilation as a function of  $M_{H_0}$ . The higgs mass  $M_h$  is fixed at 120 GeV. *Left panel:*  $\mu_2 = 40$  GeV; *Right panel:*  $\mu_2 = 200$  GeV.

## 4 Dark Matter annihilations

IDM dark matter annihilation in the galactic halo takes place through channels that, to some extent, depend on the mass range being considered. However, in the simplest version of the model, the flux of positron (and *a fortiori* that of antiprotons) is indirect and result from other primary annihilation products, like  $W^+ - W^-$  pairs, or hadronisation processes.

This source of positrons/antiprotons is added to the diffusion equation through a term

$$Q(E, (\vec{x})) = \sum_f \langle \sigma_{\text{ann}} v \rangle_{\text{tot}} \cdot BR_f \frac{dN_f}{dE} \frac{\rho_{DM}^2(\vec{x})}{M_{DM}^2}, \quad (19)$$

where  $\langle \sigma_{\text{ann}} v \rangle_{\text{tot}}$ ,  $BR_f$  and  $\frac{dN_f}{dE}$  are respectively the total (average) annihilation cross section times the relative velocity  $v$ , the branching ratio into state  $f$  and the fragmentation function of the final state  $f$  into positrons/antiprotons.  $M_{DM}$  is the mass of the dark matter candidate. Those four quantities depend on particle physics assumptions whereas  $\rho_{DM}$  is the mass distribution of dark matter in the halo.

We have implemented the IDM in the microMEGAs2.2 code which gives the relic abundance of dark matter as a function of the model parameters. The code also gives access to the annihilation branching ratios. Depending on the mass (and parameters), annihilation takes place dominantly either through the Higgs (low and middle mass ranges) or through  $W^+ - W^-$  and  $Z - Z$  pairs (middle and high mass ranges). The resulting branching ratios are shown in Fig.1 for a Higgs mass fixed to  $M_h = 120$  GeV and two values of the  $\mu_2$  parameters,  $\mu_2 = 40$  and 200 GeV. Above 80 GeV, the  $H_0$  annihilates essentially into gauge bosons. Once  $M_{H_0} \geq M_h$ , the annihilation into  $h$  pairs opens, with a rate that is dictated by the  $H_0 - h$  coupling  $\lambda_L$ .

The difference between the two panels of Fig.1 is perhaps worth being stressed. Below the threshold for Higgs production, the BR are roughly the same. If  $M_{H_0} \sim \mu_2$  the  $\lambda_L$  is small and, since the annihilation into fermion pairs (resp. into gauge bosons) is controlled by  $\lambda_L$  (resp. gauge couplings), there is a dip in the fermion and  $hh$  branching ratios in the right panel. The behaviour of the dip in the  $hh$  channel comes from the change of the sign of  $\lambda_L$ . It is positive for  $\mu_2 < M_{H_0}$  and there is a destructive interference between the Feynman diagrams (see [14]), while for  $M_h < M_{H_0} < \mu_2$  the amplitudes add up, an effect which leads to an enhancement of the branching ratio to Higgs.

The rate of dark matter annihilation is proportional to the square of the number density  $n(\vec{r}) = \rho(\vec{r})/m_{DM}$ , whose profile is not well known. Rotation curves observations suggest a rather cored profile [54,55], with a flat behaviour at the centre, whereas numerical simulations predict more cuspy profiles in the innermost region of the Galactic centre (see Kravtsov et al. [55], Navarro-Frenk-White (NFW) [56] and Moore et al. [57] as well as the recent Via Lactea and Aquarius simulations [58, 59]). In the present study, we focus on the popular

NFW distribution which is parameterized as follow

$$\rho(r) = \rho_0 \left( \frac{r}{r_0} \right)^{-\gamma} \left[ \frac{1 + (r_0/a_0)^\alpha}{1 + (r/a_0)^\alpha} \right]^{\left( \frac{\beta-\gamma}{\alpha} \right)}, \quad (20)$$

where  $r_0$  is the Galactocentric distance and  $\rho_0 = 0.3 \text{ GeV/cm}^3$  is the dark matter density in the solar neighborhood and  $(r_0 [\text{kpc}], a_0 [\text{kpc}], \alpha, \beta, \gamma) = (8.0, 20, 1, 3, 1)$ .

On top of this smooth, averaged distribution, numerical simulations indicate that virialized system are left with surviving substructures or *clumps* of dark matter [58–63]. It has then been first suggested that such clumps can lead to orders of magnitude enhancement of the dark matter annihilation rate. This effect is parameterized through the so-called *boost factor*

$$\text{BF} = \frac{\int_V d^3x \rho_{clumpy}^2}{\int_V d^3x \rho_{smooth}^2} \cong \frac{\int_V d^3x \rho_{clumpy}^2}{\rho_0^2 V}, \quad (21)$$

where the region of integration is the volume which contributes to the annihilation flux, i.e. a few  $\text{kpc}^3$ . Recent developments tend to disfavour the existence of such enhancement of the flux [64–66] and has also shown its energy dependence [64, 65]. Furthermore, it is expected to be different for positrons than for anti-protons. Nevertheless, considering the uncertainties on this question, and following standard practice, we consider boost factors  $\text{BF} = \mathcal{O}(10 - 100)$  in this work.

Another, more controllable, source of potential enhancement of the annihilation rate has recently received much attention. It has been shown that, in presence of effectively attractive long range interactions, the annihilations of non-relativistic dark matter particles may be enhanced in the limit of small relative velocities [67]. This so-called Sommerfeld or *aka* Sakharov effect [68] may lead to large enhancements  $\mathcal{O}(10 - 10^3)$  of the annihilation cross sections. A general analysis of Sommerfeld enhancement is complex [67] but, the rule of thumb is that this effect might be relevant for heavy dark matter candidates. More precisely, the large mass IDM case is very much analogous to the Minimal Dark Matter scenario, provided  $M_{DM} \gtrsim M_W/\alpha_W$ , with  $W$  boson exchange giving effectively long range interactions with enhancements of  $\mathcal{O}(10^2)$  [69]. For the low and middle mass range, Sommerfeld enhancement can not be invoked.

## 5 The IDM *vs* the PAMELA, ATIC and HESS observations

The PAMELA satellite has published its first scientific results on  $e^+$  and  $\bar{p}$  in Fall 2008 [20]. The primary goal of PAMELA is the study of the antimatter component of moderate energy cosmic rays, with better resolution and, being a satellite and not a balloon experiment, with far better statistics than previous experiments.

Concerning positrons, AMS 98 [70] and balloon experiments like CAPRICE 94 [71], CAPRICE 98 [49] and HEAT 00 [72] have taken data between 300 MeV and 40 GeV. PAMELA has been designed to extend this range from 50 MeV to 270 GeV. The present data published so far cover the range between about 2 and 80 GeV (see Fig.2, left), corresponding to about  $10^4$  positrons identified [20].

The PAMELA collaboration has not yet released their observations of absolute flux of  $e^-$  and  $e^+$ , but the PPB-BETS, ATIC and HESS collaborations have measured the flux of electrons in the energy range 30 GeV - 4 TeV [23, 73, 74]. Unlike PAMELA, this experiment can not distinct electrons from positrons, hence in principle their data may also include positrons, Fig.2, middle. The same figure also displays the recent HESS observations.

The antiproton fluxes have been analyzed by IMAX 92 [75], BESS 95+97 [76] BESS 99 [77], BESS 02 [78], BESS Polar [79], CAPRICE 98 [80] and HEAT 00 [81] experiments from 120 MeV to 40 GeV. PAMELA is designed to improve this measurement from 80 MeV to 190 GeV. The present published data give the  $\bar{p}/p$  ratio up to 100 GeV, corresponding to about  $10^3$   $\bar{p}$  identified, Fig.2, right [21, 53]. Ultimate measurements of PAMELA will be achieved with high statistics, with  $10^5$  and  $10^4$  events after three years of operation for positrons and antiprotons respectively. The data displayed in Fig.2 are compared with the expected backgrounds, (8-9) and (14-16). For anti-protons there is good agreement between expectations and observations but the positrons and electrons data show significant deviations.

The PAMELA data show a depletion of the  $e^+$  fraction below 5 – 6 GeV compared with previous experiments. The discrepancy is not fully understood yet, but as discussed above it is assumed to be due to a

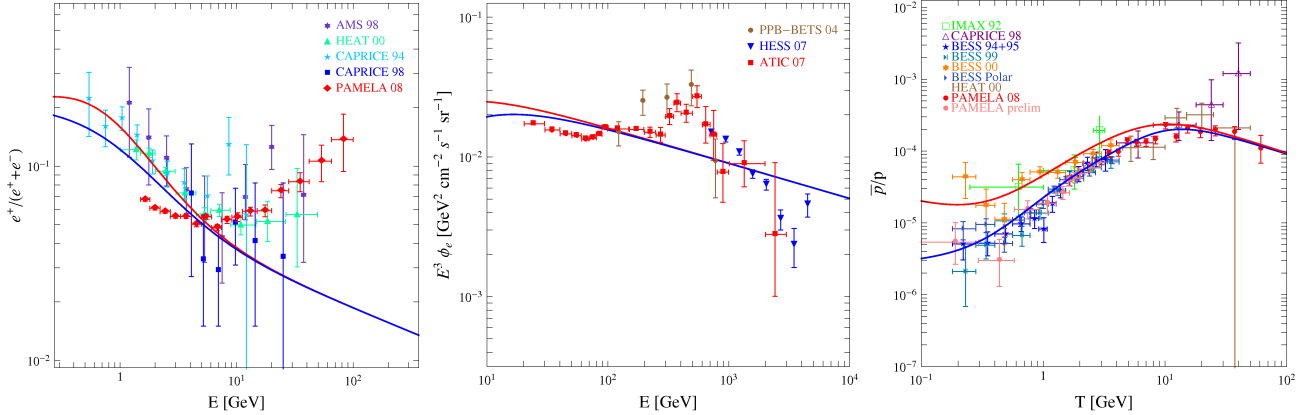


Figure 2: *Left panel*: Positron fraction measured by balloon experiments and PAMELA (in red). *Centre panel*: Total electron+positron flux measured by balloon experiments together with the HESS data. *Right panel*:  $\bar{p}/p$  fraction. In all cases the red (blue) line represent the expected background from Eq. (13-15). and Eq. (8-9) for leptons and baryons respectively without (with) a solar modulation of  $\phi = 500$  MV.

charge dependent solar modulation effect related to the periodic inversion in the solar magnetic field. Naively we could expect an anti-correlation in time between the positron and anti-proton data (*ie* minima of positron fraction corresponding to maxima of  $\bar{p}/p$  ratio) but, this is not what data on anti-proton, Fig. 2. However, simulations show that light and heavy particles are affected differently [52]. This is manifest in the Fig.2 of [52], which shows that both the  $e^+$  fraction and  $\bar{p}/p$  ratio should be low at the time of PAMELA data taking, which is in agreement with observations (see also the talk by S. Ricciarini at [53])

The PAMELA data also show a steadily increasing of the  $e^+$  fraction above  $\sim 10$  GeV. The standard expectation, based on simulations of  $e^+$  production through spallation and propagation in the ISM, is that the  $e^+$  fraction should decrease instead of increasing with energy. This is manifest in the expected flux of Eq.(14-16) which give

$$\left. \frac{e^+}{e^+ + e^-} \right|_{\text{bckg}} \propto E^{-0.15}$$

The data (focusing on the three high energy points, see Fig. (3) gives

$$\left. \frac{e^+}{e^+ + e^-} \right|_{\text{PAMELA}} \propto E^{0.55}$$

This excess is the cause of the recent excitement around the PAMELA data, a possible explanation being it is due to dark matter particles annihilating in the vicinity of the solar system. Furthermore it is tempting to correlate the PAMELA excess to the excess of electrons+positrons observed by ATIC at energies in the 300 – 800 GeV range. This excess is consistent with the HESS data.

In that respect, it is remarkable that if we extrapolate the PAMELA excess into an excess of both electrons and positrons (using a simple power law flux,  $\Phi_{e^-,e^+} \propto E^{-2.1}$ ), the excess in PAMELA and ATIC may be put in correspondence, Fig. 3. This is consistent with the astrophysics explanation which posits that the positrons excesses may be due to (observed or yet to be discovered) nearby pulsars [82]. Explaining both PAMELA and ATIC data from dark matter annihilation is more challenging. As discussed extensively in the recent litterature, the culprit of both excesses could be a heavy dark matter particle candidate, annihilating or decaying (in the case of a long-lived dark matter candidate), preferably in leptons.

In the present section we confront the IDM dark matter candidate to the positron and anti-proton data.



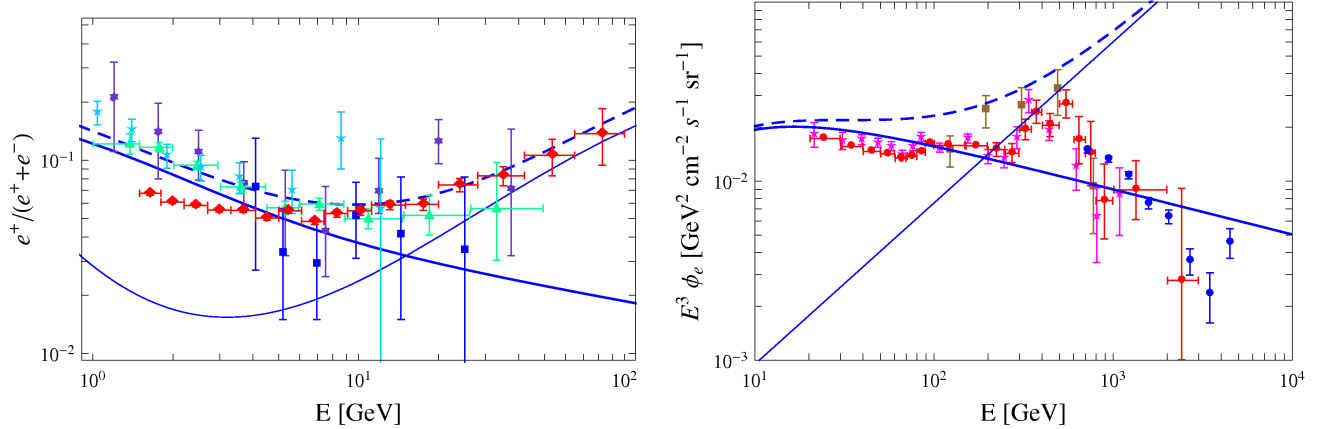


Figure 3: *Left panel* : The thin curve represent the positron fraction generated by a fiducial flux of positron  $\Phi(E) = 6.5 \cdot 10^5 E^{-2.1} \text{ GeV}^{-1} \text{ cm}^{-2} \text{ s}^{-1} \text{ sr}^{-1}$ . The thick (dashed) lines represent the background (total) positron fraction. *Right panel* : Expected total electron plus positron flux in comparison with the ATIC measurements. The lines have the same signification as in the left panel

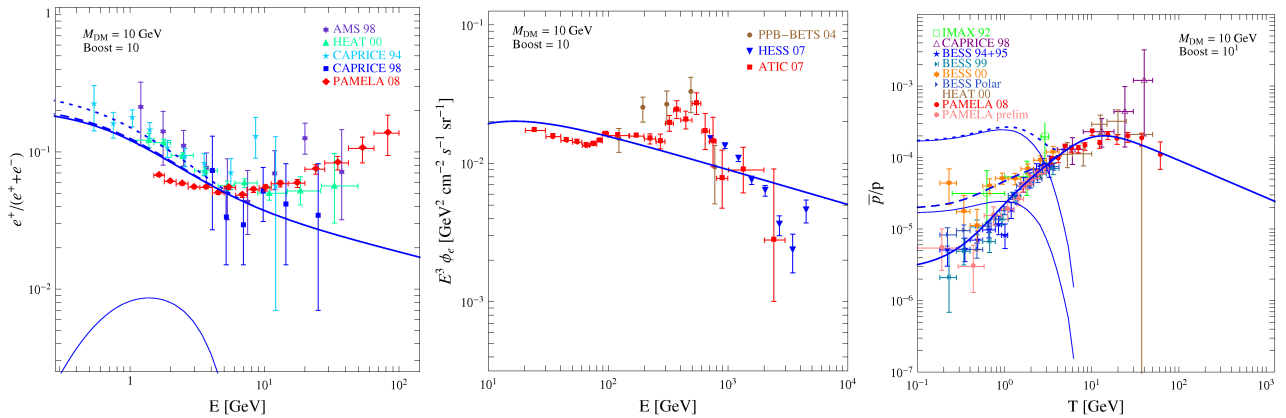


Figure 4: A Low Mass candidate ( $M_{DM} = 10 \text{ GeV}$ ). *Plain*: Background, *Dashed*: Signal + BckGrd and *Dotted*: Signal + BckGrd with boost factor = 10. Signal only are represented by light plain curves. A solar modulation of  $\phi = 500 \text{ MV}$  has been applied.

## 5.1 Low mass range

In [17] it has been shown that the IDM dark matter candidate may be consistent with both WMAP and the DAMA/LIBRA, a direct detection experiment that has reported further evidence for an annual modulation of the nuclear recoils in their detector [83]. Taking into account the null results of other DM detection experiments and the channelling effect on the threshold energy in DAMA points toward to a nuclear recoil due to dark matter-nucleon scatterings with dark matter mass in the range (see [84])

$$3 \text{ GeV} \lesssim M_{DM} \lesssim 8 \text{ GeV}$$

The best fit to DAMA/LIBRA data points to a somewhat larger mass  $M_{DM} \sim 10 - 12 \text{ GeV}$ , but these masses are within the CDMS and Xenon exclusion limits [85, 86]. At such low mass, annihilation of the  $H_0$  and its scattering with a nucleus takes place through the Higgs particle with both cross section scaling as  $\sigma \propto \lambda_L^2/m_h^4$ . For a given DM mass, imposing WMAP abundance fixes all the relevant parameters of the model (modulo some residual uncertainty in the Higgs-nucleus couplings). That agreement with DAMA/LIBRA which may

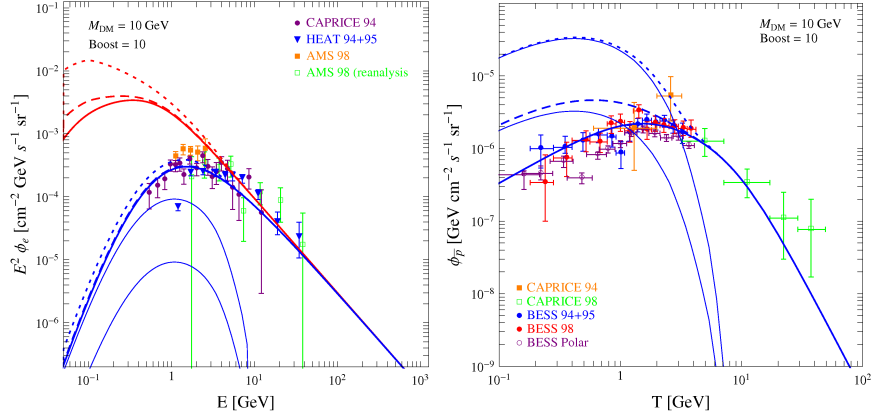


Figure 5: *Left panel (Right panel)* : Flux of positrons (antiprotons) for  $M_{DM} = 10$  GeV. *Plain*: Background, *Dashed*: BckGrd + Signal and *Dotted*: BckGrd + Signal with boost factor = 10. Red (blue) curves corresponds to signals without (with) solar modulation ( $\phi = 500$  MV). *Light Plain* curves are signal only.

be reached without further tuning is thus remarkable. This is specific to the IDM and, more generally to models with a *scalar* DM candidate coupled through the Higgs portal [17].

In our discussion of positron and anti-proton signatures we consider as benchmark a candidate with mass  $M_{DM} = 10$  GeV,  $\sigma_{SI} \approx 3 \cdot 10^{-41}$  cm<sup>2</sup>. This candidate is intermediate between the range allowed/not excluded by all experiments and the best fit to DAMA/LIBRA data. Moreover the version of DarkSUSY code we have adapted does not give the flux of positrons and anti-protons for dark matter candidates with mass below 10 GeV. Computing the flux for the whole DAMA/LIBRA range would require to update the Pythia tables of DarkSUSY toward lower masses but we have not yet done so. We do not expect much difference between a 10 GeV and an 8 GeV candidates. Lower mass candidate, say  $M_{DM} \sim 4$  GeV, could give larger flux (albeit at lower energies) but these candidate are less favoured by the DAMA/LIBRA data so, at this exploratory level, we limit ourself to a candidate with  $M_{DM} = 10$  GeV.

Cosmic abundance consistent with WMAP is reached for  $\lambda_L \approx -0.2$  for  $M_h = 120$  GeV and  $M_{DM} = 10$  GeV. Then the flux of positrons and anti-protons is fixed modulo the usual uncertainties regarding the distribution of dark matter in the halo and the propagation parameters. The results are given in Fig.4. In all three figures, the dashed line correspond to a candidate with standard NFW distribution, while the dotted line correspond to a signal boosted by a factor of 10. Given the low mass of the  $H_0$ , the signal is in the range of energies where both the positron and anti-proton fluxes are subject to solar modulation, which complicates the comparison between theoretical predictions and data.

For both positrons and anti-protons, the contamination by dark matter annihilations is consequent only if we allow for some boost in the signal, here  $BF = 10$ . Also the effect is the most dramatic for anti-protons. This is essentially because the background signal is expected to be much smaller for  $\bar{p}/p$  than for the positron fraction. Focusing on positrons, the excess may be somewhat attenuated by playing with the rigidity parameter  $\phi$  (we have used  $\phi = 500$  MeV in the plots) but doing so would also affect all low energy cosmic rays fluxes (including larger  $Z$  components) so we have refrained doing so. This leaves open the possibility of hiding the dark matter signal with a charged dependent solar modulation effect (provided the boost factor is not too large). It remains to be seen whether this can be done in a consistent way for all cosmic ray components, which differ in mass or charge. Moreover, dark matter annihilates into fermion-antifermion pairs and so an excess would be also be manifest in absolute fluxes. These are shown in Fig.5 for positrons and anti-protons, together with existing data AMS 98 [70], CAPRICE 94 [71], CAPRICE 98 [87], BESS 95+97 [30], BESS 98 [88] and BESS Polar [79]. For lack of a systematic analysis of solar modulation in the light of recent data, for the time being, it is probably fair to conclude that boosts larger than  $BF = 1$  are excluded from anti-protons data alone. We expect constraints from positrons to remain much milder, since the DM contribution is clearly smaller than the overall effect of solar modulation. Notice that  $BF = 10$  is quite a large boost factor, *a fortiori* for anti-protons which may travel much greater distances without losing

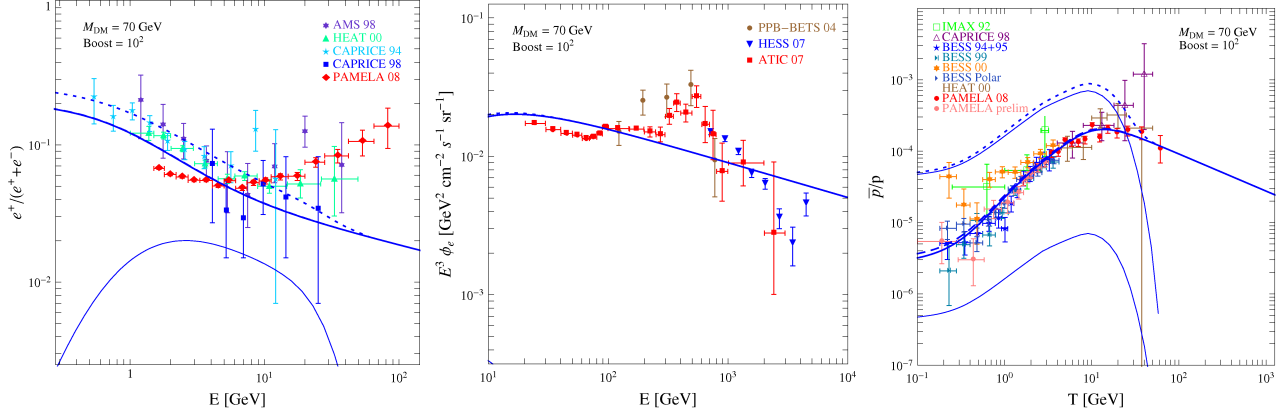


Figure 6: Same as Fig. 4 but for a Middle Mass candidate ( $M_{DM} = 70$  GeV,  $BF = 10^2$ ).

energy than positrons may. The antiproton (resp. positron) high (resp. low) energy part of the fluxes are thus less subject to local fluctuations in the distribution of dark matter [66]. This implies also that the boost may be different for positrons and anti-protons [65].

To conclude the discussion on a light IDM dark matter candidate, we briefly comment on the production of anti-deuteron. The production of anti-deuteron by spallation is small and is predicted to fall off for kinetic energies below 1 GeV per nucleon. Given their abundance, light WIMPs may give interesting contribution to the flux of anti-deuteron at low energies (see for instance [89]). For the IDM candidate with  $M_{DM} = 10$  GeV, we get using the DarkSUSY routines an anti-deuteron flux at  $T_{\bar{D}} = 0.25$  GeV/n of  $9 \cdot 10^{-7}$  (GeV/n s sr  $m^2$ ) $^{-1}$  (for  $BF = 1$ ), below the first upper limit of  $1.9 \cdot 10^{-4}$  (GeV/n s sr  $m^2$ ) $^{-1}$  set by the BESS experiment [90], but above the expected acceptance of the future AMS-02 and GAPS experiments [91, 92], which are  $4.5 \cdot 10^{-7}$  (GeV/n s sr  $m^2$ ) $^{-1}$  and  $1.5 \cdot 10^{-7}$  (GeV/n s sr  $m^2$ ) $^{-1}$  respectively. Anti-deuteron data might thus give the strongest constraint on light IDM WIMP dark matter candidate.

## 5.2 Middle mass range

In this subsection, we consider dark matter candidates in a mass range such that not only annihilations through the Higgs but also co-annihilation through the Z are relevant to fix the relic abundance [9, 14]

$$40 \text{ GeV} \lesssim M_{DM} \lesssim 80 \text{ GeV}.$$

An illustration of this range is given in Fig. 6 where the fluxes and fractions from the annihilation of a 70 GeV candidate that has a cosmic abundance in agreement with WMAP.

Since annihilations produce dominantly  $b - \bar{b}$  pairs, the positron spectrum emerging is very soft. Even if one considers a large boost factor to bring the signal within the PAMELA level ( $BF = 10^2$  in the figure), the spectrum at the Earth can not exhibit the steep increase in the positron observed by the experiment. There is a slight excess of positrons below 10 GeV but it is consistent with observations. Moreover this is within the energy range where solar modulation is effective. However, there is again a more significant excess of  $\bar{p}$ . Although the signal may be mimicked by solar modulation for moderate boost factors, large boost factors (say  $BF \gtrsim 10^2$ ) may be clearly excluded. There is also a small excess around 10 GeV that perhaps could be probed with better statistics.

All these fluxes have been computed for  $M_h = 120$  GeV. However it is of interest to envision larger Higgs masses, since this is one of the motivations for the IDM. In [9] it has been shown that  $M_H \sim 500$  GeV may be consistent with LEP precision measurements. Although one expects that the annihilation cross section to be small for such a large Higgs mass, in [15] it has been shown that an abundance in agreement with WMAP may be reached through co-annihilation. As a bonus, just at the threshold for  $W$  pair production, which is characteristic of the middle mass range, in the limit of large Higgs mass, there is a relative enhancement of loop effects and the dark matter candidate may have annihilations channels with substantial branching ratio

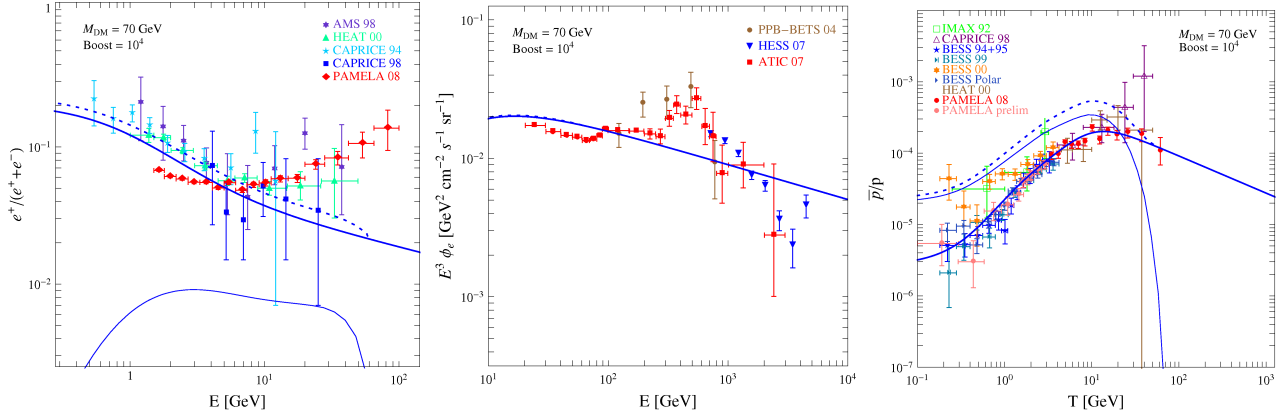


Figure 7: Same as Fig. 4 but a Middle Mass candidate ( $M_{DM} = 70 \text{ GeV}$ ,  $BF = 10^4$ ) with one-loop  $\gamma - Z$  contribution

into  $\gamma$  pairs and into  $\gamma - Z$ , a signal which could be accessible to the GLAST/Fermi satellite. Although these features come with some amount of fine tuning, this prediction is quite specific of the IDM. Since a  $Z$  may decay into lepton pairs, it is thus fair to ask whether loop effects may also enhance the production of positrons. To address this question, we have considered the Model I of [15] and have simply considered the contribution from  $Z$  decay products. At one-loop there is also a direct contribution with  $\bar{l}l\gamma$  annihilations [30], but we have neglected it for our estimate. This is legitimated by the fact that the signal is not spectacular, unless the boost factor is very large  $BF \sim 10^4$ , as shown in Fig.7. Although the shape of the spectrum is slightly harder for  $E \lesssim M_{DM}$  than it is at three level, loop effects may not reproduce the observed excesses and, at best, we could constrain the BF of the IDM dark matter candidate.

### 5.3 High mass range

For heavier dark matter particles, gauge annihilation channels become predominant. In the IDM, we may consider dark matter candidate in the mass range

$$500 \text{ GeV} \lesssim M_{DM} \lesssim 15 \text{ TeV},$$

where the upper bound comes from unitarity limit. In [14] it has shown that WMAP cosmic abundance requires  $\mu_2$  to be close to  $M_{H_0}$  and thus for most the parameter space annihilations are essentially into  $W^+ - W^-$  and  $Z$ , like for Minimal Dark candidates [11]. Fig. (8), (9) and (10) illustrate the typical signals one may expect from candidates with masses  $M_{DM} = 1, 2$  and  $10 \text{ TeV}$ . Note that, in this case, we have used an isothermal profile, so as not to contradict constraints coming from synchrotron radiation emission by dark matter annihilation products [28]. ATIC balloon experiment shows an excess between 300 and 800 GeV which may be interpreted as an excess in both positrons and electrons. This excess is consistent with the first data points of HESS. It is tempting to associate those signals to annihilation of dark matter particles of masses around TeV. This requires a large boost factor  $BF \sim 10^3$ , however, as for Minimal Dark matter, this boost may come from a combination of astrophysics and particle physics effects, the latter in the form of Sommerfeld enhancement. This being assumed, the strongest constraint comes again from  $\bar{p}$  PAMELA data which require the candidate to have a small branching ratio to baryons (see *eg* [24]) or, focusing on the IDM, to be heavier than 10 TeV (Fig.10). Unfortunately (and as well appreciated by now) the fit to ATIC/HESS is then quite poor.

One may envision improving a fit to data by extending the IDM by adding more particles, so as to have direct annihilation channels into charged lepton pairs<sup>2</sup>. However for a scalar DM candidate like in the IDM,

<sup>2</sup>The simplest and most natural extension of the IDM is to add heavy singlet neutrinos with odd parity [8] but this model does not lead to charged lepton pair annihilation channels. A possibly interesting alternative might be to embed the IDM in a Universal Extra Dimension (UED) model (see for instance [6]), in which case annihilations in charged lepton pairs are permitted.

these processes would be p-wave or chirality  $\propto m_f^2$  suppressed and thus not very useful to explain the excesses.

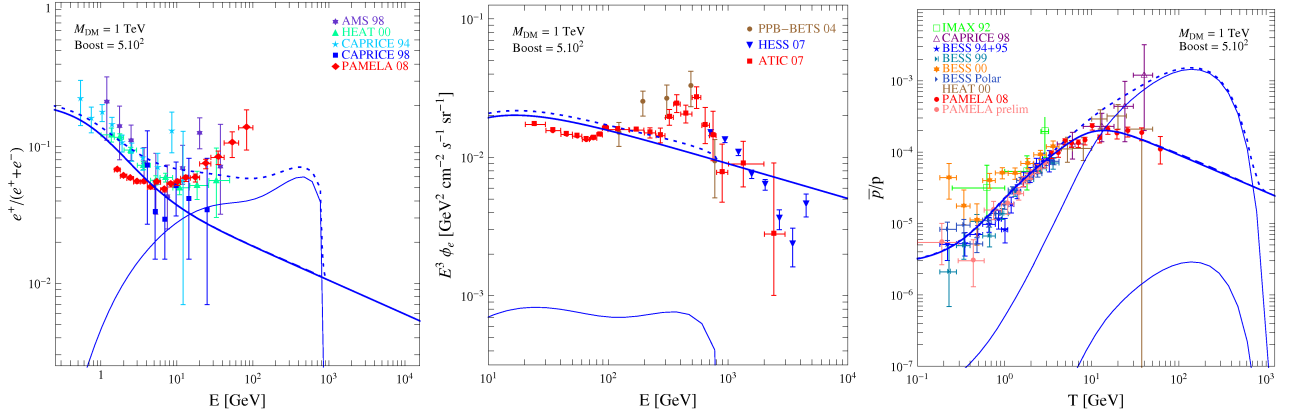


Figure 8: Same as Fig. 4 but for a High Mass candidate ( $M_{DM} = 1 \text{ TeV}$ ,  $\text{BF} = 5.10^2$ ).

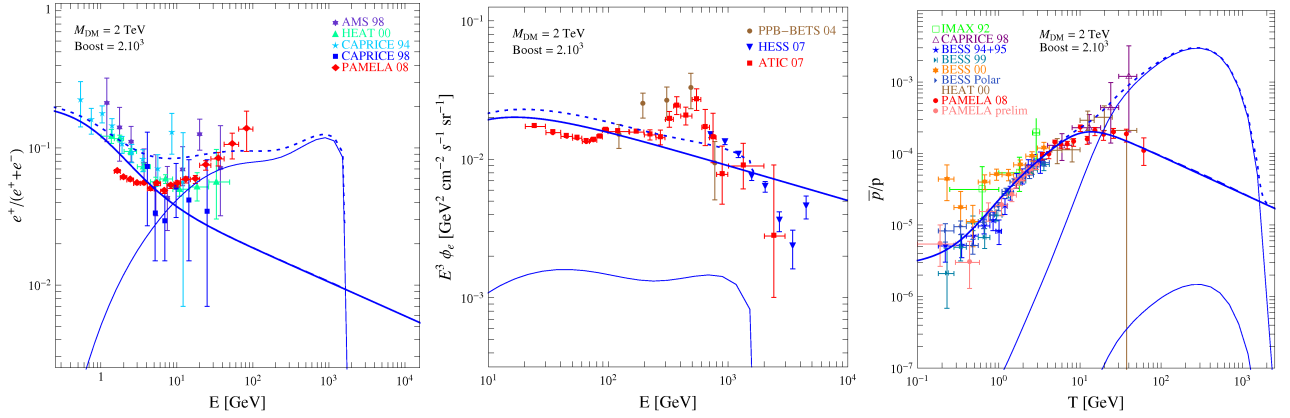


Figure 9: Same as Fig. 4 but for a High Mass candidate ( $M_{DM} = 2 \text{ TeV}$ ,  $\text{BF} = 2.10^3$ ).

## 6 Conclusion

We have confronted the IDM scalar dark matter candidate to recent data on antimatter in cosmic rays. The fit to data are generically poor compared to other, albeit more complex, dark matter candidates. The most promising possibility in that respect is to consider a very heavy DM candidate, with  $M_{DM} \gtrsim 10 \text{ TeV}$ , so as to evade constraints from the anti-protons flux but at the price of a large boost factor. In that respect, the predictions of the IDM are similar to those of Minimal Dark Matter candidates, which is not surprising, given that the branching ratio into  $W^+ - W^-$  and  $Z$  pairs are large in both models. Similarly, although we have not computed the effect, it may be expected that Sommerfeld enhancement is similar in both models. In many respects, the most interesting feature of the model is the large flux of positrons, anti-protons, and anti-deuterons that may arise in the case of rather light dark matter candidate. This comes essentially from two trivial features, the first being that the annihilation rate is large and dominated by Higgs exchange, the second being that the flux is proportional to the number density squared, which is large (actually similar to the cosmic abundance of ordinary matter) for a candidate with  $M_{DM} \lesssim 10 \text{ GeV}$ . As a consequence, the flux of anti-deuteron is predicted to be above the expected AMS-02 sensitivity. One issue in confronting such

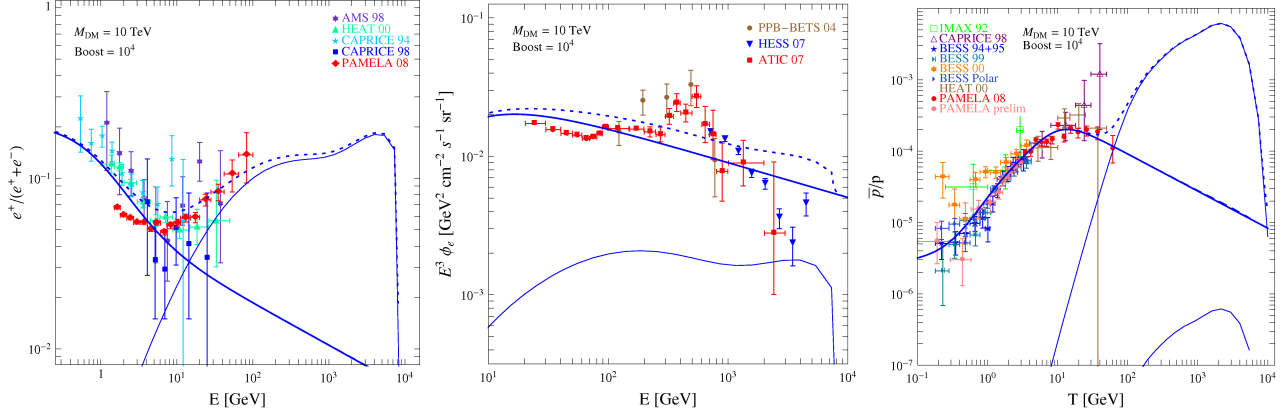


Figure 10: Same as Fig. 4 but for the High Mass regime ( $M_{DM} = 10 \text{ TeV}$ ,  $\text{BF} = 10^4$ ).

candidates to observations is that low energy cosmic rays are sensitive to solar modulation, which needs to be better understood. If so, our impression is that useful constraints might be put on the properties of light dark matter candidates,  $M_{DM} \lesssim 10 \text{ GeV}$ , a category that encompasses many models.

## Acknowledgments

The work of G. Vertongen and M.H.G. Tytgat is supported by the FNRS and Belgian Federal Science Policy (IAP VI/11).

## References

- [1] E. Komatsu *et al.* [WMAP Collaboration], arXiv:0803.0547 [astro-ph].
- [2] U. Seljak, A. Slosar and P. McDonald, JCAP **0610** (2006) 014.
- [3] W. M. Yao *et al.* [Particle Data Group], J. Phys. G **33** (2006) 1.
- [4] G. Jungman, M. Kamionkowski and K. Griest, Phys. Rept. **267**, 195 (1996) [arXiv:hep-ph/9506380].
- [5] G. Bertone, D. Hooper and J. Silk, Phys. Rept. **405** (2005) 279 [arXiv:hep-ph/0404175].
- [6] D. Hooper and S. Profumo, Phys. Rept. **453** (2007) 29 [arXiv:hep-ph/0701197].
- [7] N. G. Deshpande and E. Ma, Phys. Rev. D **18** (1978) 2574.
- [8] E. Ma, Phys. Rev. D **73** (2006) 077301.
- [9] R. Barbieri, L. J. Hall and V. S. Rychkov, Phys. Rev. D **74** (2006) 015007 [arXiv:hep-ph/0603188].
- [10] T. Hambye and M. H. G. Tytgat, Phys. Lett. B **659** (2008) 651 [arXiv:0707.0633 [hep-ph]].
- [11] M. Cirelli, N. Fornengo and A. Strumia, Nucl. Phys. **B753** (2006) 178.
- [12] J. McDonald, Phys. Rev. D **50** (1994) 3637 [arXiv:hep-ph/0702143].
- [13] B. Patt and F. Wilczek, arXiv:hep-ph/0605188.
- [14] L. Lopez Honorez, E. Nezri, J. F. Oliver and M. H. G. Tytgat, JCAP **0702** (2007) 028
- [15] M. Gustafsson, E. Lundstrom, L. Bergstrom and J. Edsjo, arXiv:astro-ph/0703512.
- [16] D. Majumdar and A. Ghosal, arXiv:hep-ph/0607067.
- [17] S. Andreas, T. Hambye and M. H. G. Tytgat, arXiv:0808.0255 [hep-ph].
- [18] P. Agrawal, E. M. Dolle and C. A. Krenke, arXiv:0811.1798 [hep-ph].
- [19] M. Taoso, G. Bertone and A. Masiero, JCAP **0803** (2008) 022 [arXiv:0711.4996 [astro-ph]].

- [20] O. Adriani *et al.*, arXiv:0810.4995 [astro-ph].
- [21] O. Adriani *et al.*, arXiv:0810.4994 [astro-ph].
- [22] J. Chang *et al.*, Nature **456** (2008) 362.
- [23] H. E. S. S. Collaboration, arXiv:0811.3894 [astro-ph].
- [24] M. Cirelli, M. Kadastik, M. Raidal and A. Strumia, arXiv:0809.2409 [hep-ph].
- [25] V. Barger, W. Y. Keung, D. Marfatia and G. Shaughnessy, arXiv:0809.0162 [hep-ph].
- [26] F. Donato, D. Maurin, P. Brun, T. Delahaye and P. Salati, arXiv:0810.5292 [astro-ph].
- [27] I. Cholis, G. Dobler, D. P. Finkbeiner, L. Goodenough and N. Weiner, arXiv:0811.3641 [astro-ph].
- [28] G. Bertone, M. Cirelli, A. Strumia and M. Taoso, arXiv:0811.3744 [astro-ph].
- [29] M. Cirelli and A. Strumia, arXiv:0808.3867 [astro-ph].
- [30] L. Bergstrom, T. Bringmann and J. Edsjo, arXiv:0808.3725 [astro-ph].
- [31] N. Arkani-Hamed, D. P. Finkbeiner, T. Slatyer and N. Weiner, arXiv:0810.0713 [hep-ph].
- [32] E. Lundstrom, M. Gustafsson and J. Edsjo, arXiv:0810.3924 [hep-ph].
- [33] Q. H. Cao, E. Ma and G. Rajasekaran, arXiv:0708.2939 [hep-ph].
- [34] P. Chardonnet, G. Mignola, P. Salati and R. Taillet, Phys. Lett. B **384** (1996) 161 [arXiv:astro-ph/9606174].
- [35] A. Bottino, F. Donato, N. Fornengo and P. Salati, Phys. Rev. D **58**, 123503 (1998) [arXiv:astro-ph/9804137].
- [36] I. V. Moskalenko, A. W. Strong, J. F. Ormes and M. S. Potgieter, Astrophys. J. **565**, 280 (2002) [arXiv:astro-ph/0106567].
- [37] L. Bergstrom, J. Edsjo and P. Ullio, Astrophys. J. **526**, 215 (1999) [arXiv:astro-ph/9902012].
- [38] P. Gondolo, J. Edsjo, P. Ullio, L. Bergstrom, M. Schelke and E. A. Baltz, JCAP **0407**, 008 (2004) [arXiv:astro-ph/0406204].
- [39] G. Belanger, F. Boudjema, A. Pukhov and A. Semenov, arXiv:0803.2360 [hep-ph].
- [40] G. Belanger, F. Boudjema, A. Pukhov and A. Semenov, Comput. Phys. Commun. **177** (2007) 894.
- [41] T. Bringmann and P. Salati, Phys. Rev. D **75** (2007) 083006 [arXiv:astro-ph/0612514].
- [42] A. M. Lionetto, A. Morselli and V. Zdravkovic, JCAP **0509**, 010 (2005) [arXiv:astro-ph/0502406].
- [43] E. A. Baltz and J. Edsjo, Phys. Rev. D **59** (1999) 023511 [arXiv:astro-ph/9808243].
- [44] T. Delahaye, F. Donato, N. Fornengo, J. Lavalle, R. Lineros, P. Salati and R. Taillet, arXiv:0809.5268 [astro-ph].
- [45] D. Casadei and V. Bindi, Astrophys. J. **612** (2004) 262.
- [46] I. V. Moskalenko and A. W. Strong, Astrophys. J. **493** (1998) 694 [arXiv:astro-ph/9710124].
- [47] L. J. Gleeson and W. I. Axford, Astrophys. J. **149** (1967) L115.
- [48] L. J. Gleeson and W. I. Axford, Astrophys. J. **154** (1968) 1011.
- [49] M. Boezio *et al.*, *Prepared for 26th International Cosmic Ray Conference (ICRC 99), Salt Lake City, Utah, 17-25 Aug 1999*
- [50] S. W. Barwick *et al.* [HEAT Collaboration], Astrophys. J. **482** (1997) L191 [arXiv:astro-ph/9703192].
- [51] M. A. DuVernois *et al.*, Astrophys. J. **559** (2001) 296.
- [52] J. Clem and P. A. Evenson, *Prepared for 28th International Cosmic Ray Conferences (ICRC 2003), Tsukuba, Japan, 31 Jul - 7 Aug 2003*
- [53] S. Ricciarini, *Talk given at the french workshop on supersymmetry (GDR SUSY), Orsay, 3-4 Dec 2008.* <http://indico.lal.in2p3.fr/conferenceDisplay.py?confId=528>
- [54] R. A. Flores and J. R. Primack, Astrophys. J. **427** (1994) L1 [arXiv:astro-ph/9402004].

- [55] A. V. Kravtsov, A. A. Klypin, J. S. Bullock and J. R. Primack, *Astrophys. J.* **502**, 48 (1998) [arXiv:astro-ph/9708176].
- [56] J. F. Navarro, C. S. Frenk and S. D. M. White, *Astrophys. J.* **462**, 563 (1996) [arXiv:astro-ph/9508025].
- [57] B. Moore, S. Ghigna, F. Governato, G. Lake, T. R. Quinn, J. Stadel and P. Tozzi, *Astrophys. J.* **524** (1999) L19.
- [58] V. Springel *et al.*, arXiv:0809.0898 [astro-ph].
- [59] J. Diemand, M. Kuhlen, P. Madau, M. Zemp, B. Moore, D. Potter and J. Stadel, arXiv:0805.1244 [astro-ph].
- [60] J. F. Navarro *et al.*, arXiv:0810.1522 [astro-ph].
- [61] J. Silk and A. Stebbins, *Astrophys. J.* **411**, 439 (1993).
- [62] J. Diemand, M. Kuhlen and P. Madau, *Astrophys. J.* **657**, 262 (2007) [arXiv:astro-ph/0611370].
- [63] J. Diemand, M. Kuhlen and P. Madau, *Astrophys. J.* **667**, 859 (2007) [arXiv:astro-ph/0703337].
- [64]
- [64] J. Lavalle, J. Pochon, P. Salati and R. Taillet, arXiv:astro-ph/0603796.
- [65] J. Lavalle, Q. Yuan, D. Maurin and X. J. Bi, arXiv:0709.3634 [astro-ph].
- [66] J. Lavalle, E. Nezri, F. S. Ling, L. Athanassoula and R. Teyssier, arXiv:0808.0332 [astro-ph].
- [67] J. Hisano, S. Matsumoto, M. M. Nojiri and O. Saito, *Phys. Rev. D* **71** (2005) 063528 [arXiv:hep-ph/0412403].
- [68] L.D. Landau and E.M. Lifshitz, “Quantum Mechanics”, Butterworth-Heinemann (1996)
- [69] M. Cirelli, A. Strumia and M. Tamburini, *Nucl. Phys. B* **787** (2007) 152 [arXiv:0706.4071 [hep-ph]].
- [70] M. Aguilar *et al.* [AMS-01 Collaboration], *Phys. Lett. B* **646**, 145 (2007) [arXiv:astro-ph/0703154].
- [71] M. Boezio *et al.* [WIZARD Collaboration], *Astrophys. J.* **532** (2000) 653.
- [72] J. J. Beatty *et al.*, *Phys. Rev. Lett.* **93** (2004) 241102 [arXiv:astro-ph/0412230].
- [73] S. Torii *et al.*, arXiv:0809.0760 [astro-ph].
- [74] J. Chang *et al.*, *Nature* **465** (2008) 362.
- [75] J. W. Mitchell *et al.*, *Phys. Rev. Lett.* **76**, 3057 (1996).
- [76] S. Orito *et al.* [BESS Collaboration], *Phys. Rev. Lett.* **84**, 1078 (2000) [arXiv:astro-ph/9906426].
- [77] Y. Asaoka *et al.*, *Phys. Rev. Lett.* **88**, 051101 (2002) [arXiv:astro-ph/0109007].
- [78] Y. Shikaze *et al.*, *Astropart. Phys.* **28**, 154 (2007) [arXiv:astro-ph/0611388].
- [79] K. Abe *et al.*, *Phys. Lett. B* **670**, 103 (2008) [arXiv:0805.1754 [astro-ph]].
- [80] M. Boezio *et al.* [WiZard/CAPRICE Collaboration], *Astrophys. J.* **561** (2001) 787 [arXiv:astro-ph/0103513].
- [81] A. S. Beach *et al.*, *Phys. Rev. Lett.* **87**, 271101 (2001) [arXiv:astro-ph/0111094].
- [82] D. Hooper, P. Blasi and P. D. Serpico, arXiv:0810.1527 [astro-ph].
- [83] R. Bernabei *et al.* [DAMA Collaboration], *Eur. Phys. J. C* **56** (2008) 333 [arXiv:0804.2741 [astro-ph]].
- [84] F. Petriello and K. M. Zurek, *JHEP* **0809** (2008) 047 [arXiv:0806.3989 [hep-ph]].
- [85] M. Fairbairn and T. Schwetz, arXiv:0808.0704 [hep-ph].
- [86] S. Chang, A. Pierce and N. Weiner, arXiv:0808.0196 [hep-ph].
- [87] M. Boezio *et al.* [WIZARD Collaboration], *Astrophys. J.* **487** (1997) 415.
- [88] T. Maeno *et al.* [BESS Collaboration], *Astropart. Phys.* **16**, 121 (2001) [arXiv:astro-ph/0010381].
- [89] F. Donato, N. Fornengo and P. Salati, *Phys. Rev. D* **62**, 043003 (2000) [arXiv:hep-ph/9904481].
- [90] H. Fuke *et al.*, *Phys. Rev. Lett.* **95**, 081101 (2005) [arXiv:astro-ph/0504361].
- [91] R. Caballero, J. C. D’Olivo, G. Medina-Tanco, L. Nellen, F. A. Sanchez, J. F. Valdes-Galicia; *Proceedings of the 30th International Cosmic Ray Conference*, Universidad Nacional Autonoma de Mexico, Mexico City, Mexico, 2008; Vol. 4 (HE part 1), pages 765-768.
- [92] H. Fuke *et al.*, *Adv. Space Res.* **41**, 2056 (2008).